IOP Publishing Measurement Science and Technology
Meas. Sci. Technol. **27** (2016) 035701 (16pp) doi:10.1088/0957-0233/27/3/035701

Inter-laboratory comparison on the size and stability of monodisperse and bimodal synthetic reference particles for standardization of extracellular vesicle measurements

Anaïs Nicolet[1], Felix Meli[1], Edwin van der Pol[2], Yuana Yuana[2], Christian Gollwitzer[3], Michael Krumrey[3], Petr Cizmar[4], Egbert Buhr[4], Jasmine Pétry[5], Noham Sebaihi[5], Bert de Boeck[5], Vincent Fokkema[6], Rob Bergmans[6] and Rienk Nieuwland[2,6]

[1] METAS, Swiss Federal Institute of Metrology, Lindenweg 50, 3084 Wabern, Switzerland
[2] AMC, Academic Medical Centre of the University of Amsterdam, Meibergdreef 9, 1105AZ Amsterdam, The Netherlands
[3] PTB, Physikalisch-Technische Bundesanstalt, Abbestrasse 2–12, 10587 Berlin, Germany
[4] PTB, Physikalisch-Technische Bundesanstalt, Bundesallee 100, 38116 Braunschweig, Germany
[5] SMD, Service Métrologie–Metrologische Dienst, SPF Economie, Bd du Roi Albert II 16, 1000 Brussels, Belgium
[6] VSL, Dutch Metrology Institute, Thijsseweg 11, Delft, The Netherlands

E-mail: felix.meli@metas.ch

Received 29 July 2015, revised 11 January 2016
Accepted for publication 13 January 2016
Published 4 February 2016

Abstract

In future, measurements of extracellular vesicles in body fluids could become a standard diagnostic tool in medicine. For this purpose, reliable and traceable methods, which can be easily applied in hospitals, have to be established. Within the European Metrological Research Project (EMRP) 'Metrological characterization of micro-vesicles from body fluids as non-invasive diagnostic biomarkers' (www.metves.eu), various nanoparticle reference materials were developed and characterized. We present results of an international comparison among four national metrology institutes and a university hospital. The size distributions of five monodisperse and two bimodal spherical particle samples with diameters ranging from 50 nm to 315 nm made out of silica and polystyrene were compared. Furthermore, the stability of the samples was verified over a period of 18 months. While monodisperse reference particle samples above a certain size level lead to good agreements of the size measurements among the different methods, small and bimodal samples show the limitations of current 'clinical' methods. All samples proved to be stable within the uncertainty of the applied methods.

Keywords: nanoparticles, extracellular vesicles, calibration, inter-laboratory comparison, bimodal size distribution

(Some figures may appear in colour only in the online journal)

1. Introduction

Many medical decisions are based on information obtained from analysis of body fluids. Body fluids contain not only cells and soluble biomolecules, but also extracellular vesicles (EV), which have a diameter ranging from 30 nm to 1 μm. Since the size, number concentration and composition of EV change with disease, including cancer, diabetes, and cardiovascular anomalies, EV comprise clinically relevant information [1]. Utilization of this information requires clinical studies, which in turn require standardization to obtain reliable reference size and number concentration values of EV. However, because reference materials and standardization procedures are currently inadequate, the reported number concentration of EV ranges from 10^4 to 10^{12} ml^{-1} in human blood plasma [2]. These numbers emphasize that the utilization of EV as disease biomarkers requires standardization. Therefore, we have developed the following roadmap: (1) acquiring knowledge on the physical properties of EV, (2) selecting and developing reference materials, (3) characterizing reference materials, (4) validating the clinical applicability of reference materials, (5) producing and distributing certified reference materials. In the next paragraph we will elaborate on this roadmap.

Physical properties of EV samples have been recently obtained [2–5]. The size distribution of EV typically follows a log-normal distribution, with most EV having a diameter $<$100 nm [2]. The number concentration of EV in body fluids is $>10^{10}$ ml^{-1} and the EV refractive index is $<$1.4 [4]. Within the relevant EV size range of 10 nm to 400 nm [3], no stable reference particles with refractive index $<$1.4 and known number concentration are available. Preferably, reference particles have a refractive index similar to EV, because most clinical detection methods are based on light scattering. Additionally, reference particles may be functionalized, for example to modify the surface charge or to add fluorescence. The broad size distribution of EV samples requires the development of both heterogeneous and monodisperse reference materials. Heterogeneous reference materials are important for the calibration of techniques that detect multiple EV simultaneously, such as dynamic light scattering [3]. Monodisperse reference materials are needed to define the size range wherein the EV number concentration is determined and to evaluate the size resolution of a measurement method. After selecting or developing reference materials that fulfil the aforementioned criteria, the particle size distribution, number concentration and refractive index need to be traceably determined. Furthermore, the minimum stability time should be studied to fix the expected useful life time. Next, the well-characterized reference materials should be tested on clinical detection methods and standardization procedures for these methods need to be developed. Ideally, after this validation step, national metrology institutes or accredited laboratories would provide certified reference materials to clinical labs to standardize EV measurements in multicentre clinical studies. However, collaborations between metrology institutes and clinical laboratories are scarce, and the current position on the roadmap is therefore between step 2 and 3.

This manuscript arises from a unique collaboration between metrology institutes and a clinical laboratory and presents the first steps to the development and application of certified reference materials to standardize EV measurements. We measured and compared the size distributions of five monodisperse and two bimodal samples within the size range of EV to validate the traceability of measurements, which is important, because earlier inter-laboratory comparisons of monodisperse samples [6–11] resulted in differences between the methods [12, 13]. However, to increase the impact to the 'real world' standardization of EV measurements, we selected polystyrene (PS) beads for their monodispersity and stability, we selected silica (SiO_2) beads for their low refractive index ($n \approx 1.44$) compared to polystyrene ($n > 1.60$) [14], we included two clinical detection methods, we present stability measurements over a period of 18 months, and we present measurements on the relative particle number concentration of populations in bimodal samples to bridge the gap between bimodal and polydisperse samples. Hitherto, such bimodal samples were used to test the size resolution of methods [15] or the size characterization of airborne nanoparticles [16].

In section 3 of this manuscript, the selected five monodisperse samples containing PS and SiO_2 beads with diameters ranging from 50 nm to 315 nm and the prepared bimodal samples are introduced. Section 4 discusses the progress of the inter-laboratory comparison, section 5 the applied measurement methods, and sections 6 and 7 the requirements and parameters used for data comparison. In section 8, samples were measured by traceable methods using different physical principles to assign method independent reference values and uncertainties. As an illustration of methods currently available in clinical laboratories, the samples were also measured by resistive pulse sensing (RPS) and particle tracking analysis (PTA), often also referred to as 'nanoparticle tracking analysis' (NTA), for which the measurement uncertainties and traceability routes are not available.

2. Particle samples

A set of five monodisperse samples of high quality particles suspension in water was selected (table 1) using the outcome of a survey [17]. The survey gathered information on commercial sources of reference particles with physical properties related to EV and considered the measurement methods, needs and requirements of the participants. The particles are made of either SiO_2 or PS having nominal diameters ranging from 50 nm to 315 nm. These diameters match the size range of EVs and the detection range of the measurement methods. The samples were made by two German producers: Microparticles GmbH, Research- and Development Laboratory and Kisker Biotech GmbH. The surface of the sample SiO_2_48 was functionalized with carboxyl groups. This functionalization was not required, but this was the best available sample with this size. METAS evaluated, ordered, decanted, bottled and sent a complete set to each participant, including all available documentation. All samples of a certain size originated from the same fabrication batch.

Table 1. Identification and nominal parameters of the 5 synthetic monodisperse particle samples as specified by the producers.

Sample id	Name	Diameter (nm)	SD (nm)	Mass conc. (mg ml^{-1})	Category #	Lot #
SiO_2_255	SiO_2-Forschungspartikel	255	10	50	SiO_2-F-0.25	SiO2-F-L1884
SiO_2_48	SiO_2-Hybridpartikel	48	3	10	SiO_2-F-0.05	SiO2 / hybrid-COOH-AR613A
PS_315	PS-Forschungspartikel	315	8	50	PS-F-0.3	PS-F-B1271
PS_147	PS-Forschungspartikel	147	7	50	PS-F-0.15	PS-F-KM59
PS_100	PS	100	-	25	PPs-0.1	GK923W

Table 2. Identification and nominal parameters of the 2 synthetic bimodal particle samples.

Sample id	Material	Diameter (nm)	Estimated nominal number conc. (ml^{-1})	Category #	Lot #
SiO_2_bim	SiO_2	142 & 177	1.1×10^{13}	SiO_2-F-0.15 SiO_2-F-0.2	SiO_2-F-L2897 SiO_2-F-L2017
PS_bim	PS	248 & 315	3.9×10^{12}	PS-F-0.25 PS-F-0.3	PS-F-KM58 PS-F-B1271

Additionally, two synthetic bimodal reference particle standards were prepared by mixing monodisperse samples in a way which was estimated to generate number concentration ratios of approximately 1 : 1 (table 2).

3. Participants and organization

Partners from 5 different institutes took part in this inter-laboratory comparison. The measuring methods used in this comparison included techniques with particles free in suspension such as small-angle x-ray scattering (SAXS), PTA and RPS, as well as techniques where the particles adhere to a surface, such as atomic force microscopy (AFM) and scanning electron microscopy in transmission mode (TSEM). The working principles of the methods will be described in the next section. The list of participants and their respective methods are summarized in table 3.

In September 2013 an identical set of 4 monodisperse samples was distributed to the participants. The comparison proceeded fully in parallel and no samples had to circulate. The measurement period was 2 months. In February 2014 the participants received three additional samples: a monodisperse sample PS_100 (table 1) and two samples with a bimodal distribution (table 2). In order to determine the long-term stability of the samples, all but the sample PS_100 (table 1), were measured again in February 2015.

Table 3. Participants and applied methods.

Participants	Acronym	Method
Amsterdam Medical Center, Amsterdam, The Netherlands	AMC	RPS
Amsterdam Medical Center, Amsterdam, The Netherlands	AMC	PTA
Physikalisch-Technische Bundesanstalt, Braunschweig, Germany	PTB	TSEM
Physikalisch-Technische Bundesanstalt, Berlin, Germany	PTB	SAXS
Dutch Metrology Institute, Delft, The Netherlands	VSL	AFM
Federale Overheidsdienst Economie, Brussels, Belgium	SMD	AFM
Swiss Federal Institute of Metrology, Wabern, Switzerland	METAS	AFM

4. Applied experimental methods

The methods applied within this comparison can be divided into three different groups: the ensemble methods such as SAXS, the single particle detection methods such as PTA and RPS and the imaging methods such as AFM and TSEM.

4.1. RPS at AMC

RPS (Izon Science Ltd, Christchurch, New Zealand) measures the resistance of particles that are driven through a nanopore (NP) [18]. Similar to the Coulter principle, the resistance is used to derive the particle dimension [19]. The frequency of particles passing the pore is used to derive the particle number concentration. In this experiment, different sizes of NP, suitable for the detection of particles in certain size ranges (NP100 = 70–200 nm; NP200 = 100–400 nm; NP400 = 200–800 nm), were used. Table 4 shows the nanopores used in each particle sample measurement. RPS was operated using a single pressure of 15 hPa. The voltage was set to 0.40–0.70 V and the stretch was adjusted until the baseline current was ~100 nA. Several carboxylated PS beads provided by the manufacturer were used following their instructions to calibrate the size and number concentration measurements using RPS. For the measurement, particle samples were diluted 1000 to 10 000-fold with phosphate-buffered saline (PBS) containing 0.6 mmol l^{-1} sodium dodecyl sulphate (SDS). This molar concentration of SDS did not change the conductivity of the PBS, and thus did not affect the particle measurement [19]. Diluted particle samples were measured with the same settings as for the calibration. Samples were analysed for 10 min. Particle size and width of the size distribution were evaluated from a Gaussian

Table 4. Nanopore sizes and camera levels used for the measurement of the different particle samples by RPS and PTA, respectively.

Particle sample	PTA Camera level	RPS Nanopore (NP)
SiO_2 _255	6	NP200
SiO_2_48	15	NP100
PS_315	6	NP400
PS_147	6	NP200
PS_100	10	NP100
SiO_2_bim	6	NP200
PS_bim	6	NP200

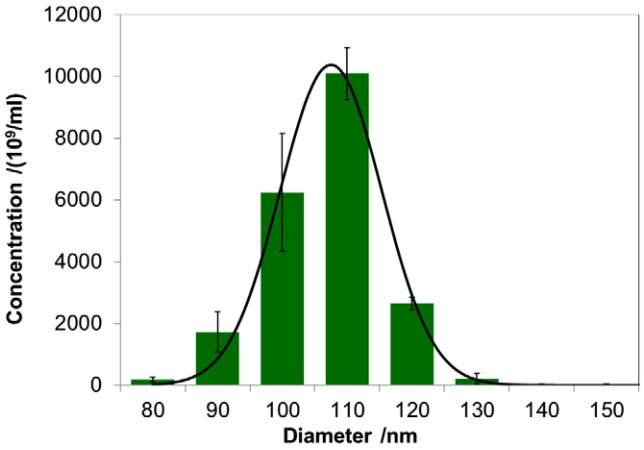

Figure 1. Size distribution evaluation of the sample PS_100 (table 1) measured by RPS. Gaussian fit (continuous line).

curve fitted to the measured size histogram. A typical analysis is shown in figure 1.

4.2. PTA at AMC

A NS500 (NanoSight Limited, London, UK) equipped with an electron multiplying charge-coupled device (EMCCD) camera (Andor Technology, Tokyo, Japan) and a 405 nm laser was used to determine the particle size distribution by tracking the Brownian motion of single particles in solution [20]. The particle size is derived from the Stokes–Einstein equation, where the mean square displacement and temperature are directly measured and the viscosity is assumed to be equal to the viscosity of water. Consequently, no calibration beads were used to calibrate the size measurements using PTA. The number concentration is derived from the mean number of scatterers in the field-of-view of the microscope (sample volume), which is calibrated by the manufacturer with 100 nm PS beads [2]. Due to a detection limit for the scattered light, the sample volume depends also on the size and the refractive index of the scattering particles. Therefore, we multiplied the number concentration as provided by the PTA software by the ratio between the expected and measured number concentration of 100 nm SiO_2 calibration beads (Silica size standards, Corpuscular, Cold Spring, NY, USA). The number concentration of 100 nm SiO_2 calibration beads was derived from the mean size (assuming spherical particles), the mass concentration and the material density as specified by the producer.

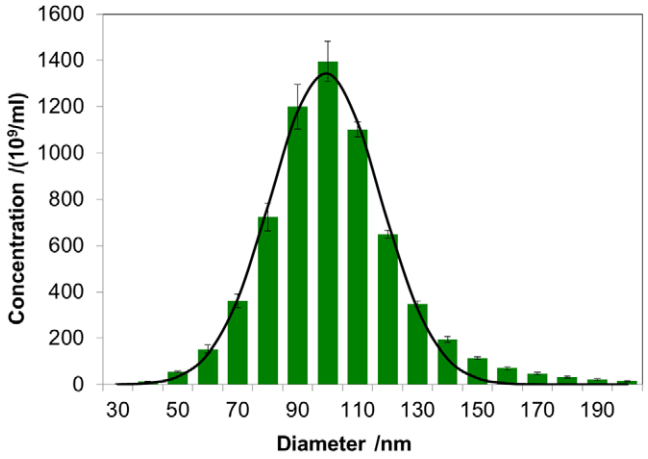

Figure 2. Size distribution evaluation of the sample PS_100 (table 1), measured by PTA. Gaussian fit (continuous line).

For the measurement, particle samples were diluted 10^4 to 10^5 fold using ultrapure water. The camera gain and camera shutter speed were set in standard mode. Several camera levels were used to measure the different particle samples (table 4). Per sample, 10 videos of 30 seconds each were captured at 22.0 °C and analysed using threshold 10 by the software PTA v2.3.0.17 (Nanosight). The size evaluation from the measured size histogram was performed the same way as for the RPS measurement. A typical analysis is shown in figure 2.

4.3. SAXS at PTB

The SAXS measurements were performed at the four-crystal monochromator beam line of PTB at BESSY II. The samples in suspension were filled into disposable borosilicate glass capillaries with an inner diameter of 1 mm and a wall thickness of 10 μm. The capillaries were sealed by welding the upper end in the flame of a propane oxygen torch. A blank sample containing only bi-distilled water was included in every batch. Each sample was used as received and in a 50% dilution with bi-distilled water to investigate possible particle interactions.

A sample holder containing the capillaries was placed into a vacuum chamber equipped with a six axes manipulator for sample movement. The synchrotron radiation was collimated using pinholes to a size smaller than 1 mm × 1 mm and focused on the sample. The incident photon flux was measured using a transmission diode located in front of the sample and the guard pinhole. A removable, calibrated diode behind the sample was used to measure the transmittance through the sample.

The scattered radiation was collected by a vacuum compatible PILATUS 1M detector [21] at a variable distance between 2 and 4.5 m behind the sample. The full set of samples was recorded in several rounds with an integration time between 100 and 360 s. The scattering images for each sample were averaged pixel-by-pixel, and the resulting images were averaged azimuthally about the beam centre to get the scattering curve.

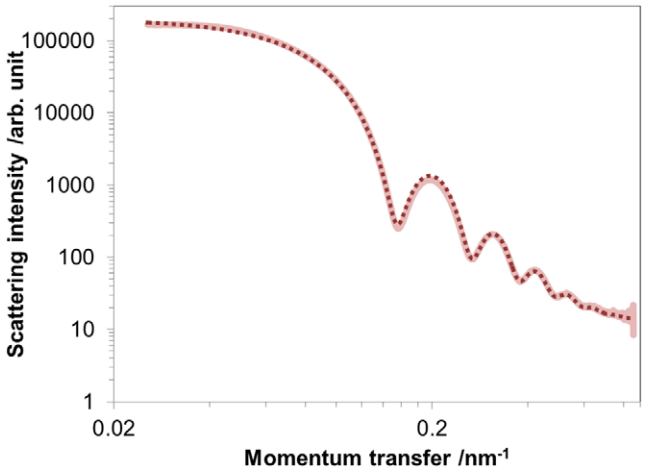

Figure 3. Scattering curve of the sample SiO_2_48 (table 1) (light continuous line) and the model curve (dark dashed line) fitted to the data.

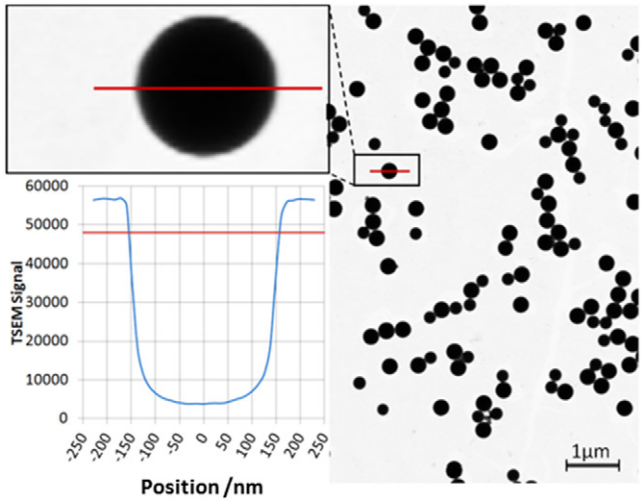

Figure 4. Example of the TSEM image of the sample PS_bim (table 2). Upper inset: 5-fold magnification of the main image showing an individual 315 nm PS particle. Lower inset shows the corresponding TSEM signal profile together with the threshold level indicating the particle boundary.

The scattering curves were normalized by the incident flux, the exposure time and the sample transmission. Figure 3 displays the resulting scattering curve for 48 nm SiO_2 particles as a function of the momentum transfer $q = 4\pi\sin\theta/\lambda$. Here, λ is the wavelength of the x-ray beam, and θ is half of the scattering angle. The wavelength is traceable to the silicon lattice constant via Bragg reflection with a relative uncertainty of 10^{-4} [22]. The scattering angle was determined from traceable measurements of the detector pixel size and the sample-to-detector distance using optical encoders with a relative uncertainty of 10^{-3} [21]. A model equation describing solid spherical particles in case of SiO_2 and core–shell particles with a stepwise constant electron density in the core and the shell in case of PS particles was fitted to the data using least-squares adjustment (dark dashed line in figure 3). The assumption of a core–shell structure for the PS particles with a light core and a thin dense shell is necessary to achieve a satisfying fit of the data as opposed to a simple solid sphere model. This has been reported earlier for similar polystyrene particles [10] and can be explained by details of the synthesis for some particles [23]. The adjustable parameters of the model were the mean particle radius, the standard deviation of the particle size distribution, the forward scattering intensity and the background intensity. For core–shell particles, two additional adjustable parameters have been used, describing the ratio of the core to shell density and the ratio of the core radius to shell thickness, which were assumed to be constant for the particle ensemble. For the bimodal mixtures, two ensembles with Gaussian size distributions and independent sets of parameters were assumed. An additive background comprising a constant and a power-law contribution was assumed.

The uncertainty of the mean particle diameter was estimated by examining the residual sum of squares χ^2 in the neighbourhood of the best fit. First, the input uncertainties were renormalized so that $\chi^2_{\mathrm{norm}} = 1$ for the best fit. Then the $1-\sigma$ confidence range of the particle diameter was determined by finding the minimum and maximum possible diameter for which $\chi^2_{\mathrm{norm}} \leqslant 2$ when all other adjustable parameters were minimized [24]. It has been shown in a previous study, that this method gives realistic uncertainty estimates for particles with narrow size distributions over a large range of particle diameters and different materials [13]. This was also the dominant uncertainty contribution. Relative uncertainty contributions related to the photon energy and the scattering angles were below 10^{-3}.

4.4. TSEM at PTB

Scanning electron microscopy in transmission mode (TSEM; Zeiss Leo Supra 35 VP) employs a conventional scanning electron microscope (SEM) equipped with an electron detector (K. E. Development, distributed by Zeiss) placed underneath the sample to register transmitted electrons. The electron detector consists of five solid state electron detectors, four of which were used as dark field detectors. The fifth detector was placed underneath a small pin hole (approximately 140 μm × 140 μm in size) and was used for bright-field imaging. Application of the bright-field detection mode provided images of the nanoparticles with better contrast than obtained with high-voltage transmission electron microscopes (TEMs), because of the larger scattering cross sections for electrons of lower energy, and standard SEMs, because the thin support film reduces substrate signal contributions. A detailed description of the measurement method is given in [25–27].

The magnification (or, equivalently pixel size) of the TSEM was calibrated by means of 2D gratings with nominal grating pitches of 144 nm and 700 nm (150-2D and 700-2D, respectively, available from Advanced Surface Microscopy Inc.) [26]. The actual grating pitch in x and y direction was calibrated at PTB using a multi-wavelength VIS/UV laser diffractometer which yields traceable values for the mean grating pitch [28, 29]. The same TSEM operating parameters were used in the calibration process and the measurement of the particle size, i.e. 30 kV acceleration voltage, 3.0 mm working

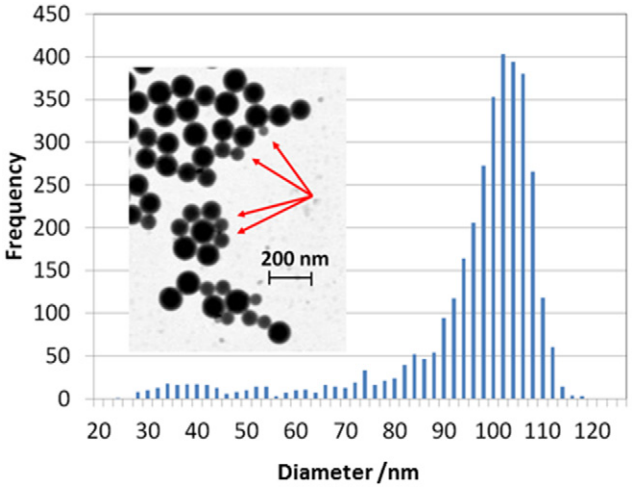

Figure 5. Size distribution measured by TSEM of the sample PS_100 (table 1). The bin size is 2 nm. Because of the asymmetric shape of the size distribution a fit using a Gaussian curve was not appropriate. The inset of the image shows a part of one of the TSEM images showing the smaller particles that are present in the sample.

distance, same magnification settings, same scan speed of the electron beam etc. Since electron microscopy measures individual distances between adjacent grating elements, a large number of individual pitch values have to be measured across the grating to determine mean pitch values with sufficient accuracy. Measurements were conducted at different spots on the grating demonstrating a sufficient homogeneity of the mean pitch across the grating. Due to leading edge distortion effects [27], for both calibration and measurement, the first 200 of the 1024 pixels along the scanning direction were omitted.

Particles under test were prepared on carbon films (TEM grids type S160, Plano GmbH). TSEM images exhibited some blurring, see TSEM signal profile shown in the inset of figure 4. This was due to two reasons: first, the number of transmitted electrons depended on the thickness of the irradiated sample which was for spheres a function of position, and second, the electron beam had a certain size leading to a corresponding image blur.

Accurate particle diameter measurements required the determination of the particle boundary from the image of the particle. An algorithm thresholds the image intensity at the appropriate border grey-level which was determined using a Monte-Carlo simulation [26, 30]. Next, all pixels corresponding to the particle were counted to determine the particle area and its area- equivalent diameter. The technique enabled automatic image analysis and was thus capable to measure a large number of particles to obtain high-resolution size distributions (figure 5).

4.5. AFM at METAS

The measurements were made using a modified Dimension 3500 metrology AFM from Digital Instruments, operating in tapping mode using standard silicon tips (42 N m^{-1}, 330 kHz). The AFM head has parallelogram flexures and uses capacitive sensors for the tip displacement measurement. The traceability to the definition of the metre of the capacitive displacement sensors was realized vertically with an interferometric z-calibration and laterally by means of reference gratings calibrated by laser diffraction at METAS. The instrument performance was verified through international BIPM[7] CCL[8] and EURAMET[9] comparisons, such as Nano2 (CCL-S2) [31], Nano4 (CCL-S1), Nano5 (CCL-S4) and EUROMET Project No 707. METAS took also part in previous nanoparticle comparisons such as within the iMERA [11] project or the APMP[10] supplementary comparison on nanoparticle size [12] with the same AFM instrument.

For each particle type the appropriate dilution (20 to 200-fold) was estimated with information from material density, particle mass concentration and size. All samples were diluted using ultrapure water. The particles were deposited on freshly cleaved, atomically flat mica surfaces. For the smallest particle sample the mica surface was beforehand treated with poly-L-lysine. After a short settling time of some seconds, most of the suspension was soaked away with the corner of a nonabrasive clean room tissue. The final drying process occurred under the light of the optical microscope.

AFM images with various ranges were made in order to check that no height information was lost due to limited image resolution (512 × 512 pixels). The scan speed and the amplitude set point were tested for their respective influence. For each type of particles several images from different locations were acquired and evaluated. All measurements were performed in a temperature controlled laboratory in the basement of METAS.

The height of the particles was measured with respect to the flat mica surface. This evaluation was performed using the particle analysis function (Particle and Pore Analysis) of the SPIP program (Image Metrology A/S, www.imagemet.com). The SPIP evaluation was verified with previously used self-made METAS AFM image evaluation software. For each particle size the results from several images were combined for the final statistical evaluation. Additional measurements of the 'Nearest Neighbours' distance (distance between the geometric centres of the actual shape and its nearest neighbour centre) were performed on samples with hexagonal closed packed layers. These results, after correction for the width of the particle size distributions, were not included in the comparison but were used to confirm the height value.

For the bimodal samples, measurements and initial evaluations were the same as for the monodisperse samples. Bimodal sample evaluations were completed by fitting a double Gaussian function to the whole size distribution histogram, in order to extract the relevant sample parameters. A typical example of a bimodal measurement and evaluation is shown in figure 6.

The uncertainty budget includes 9 contributions as described in [11]. The largest ones are the vertical calibration, the tip–sample interaction (tapping set-point) and the estimated background flatness (from both the scanner and the mica substrate).

[7] BIPM: Bureau International des Poids et Mesures.
[8] CCL: Consultative Committee for Length.
[9] EURAMET: European Association of National Metrology Institutes.
[10] APMP: Asia Pacific Metrology Programme.

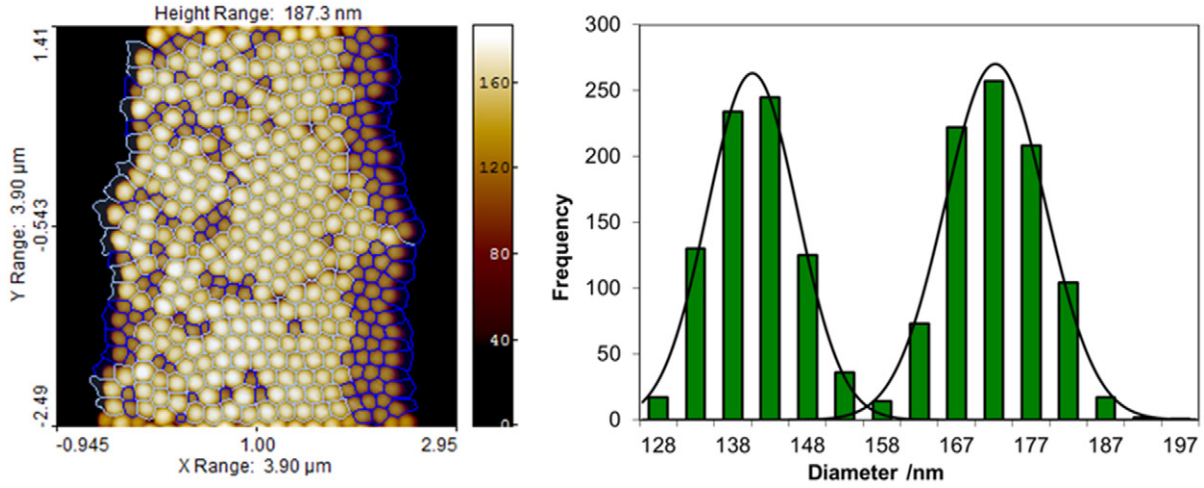

Figure 6. Left: typical AFM measurement of the sample SiO_2_bim (table 2) measured by METAS. Large particles are light coloured, while the small ones are dark coloured. Image size 3.9 μm × 3.9 μm, 512 × 512 pixels. Height evaluation using SPIP. Right: evaluation of the bimodal size distribution of the silica sample with a double Gaussian fit.

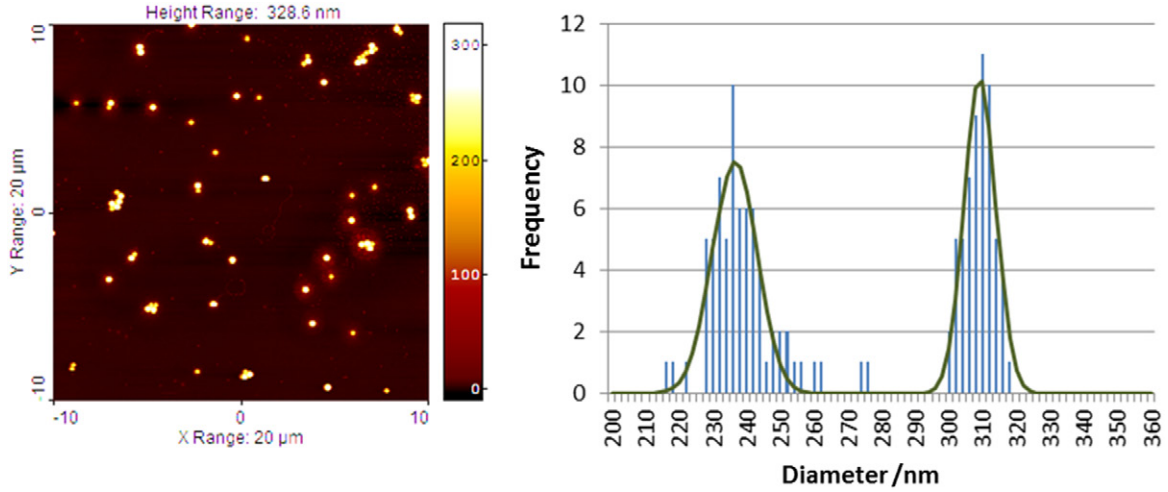

Figure 7. Left: Typical AFM measurement of the sample PS_bim (table 2) measured by SMD. Image size 20 μm × 20 μm, 512 × 512 pixels. Right: Evaluation of the bimodal size distribution of the PS_bim sample with a double Gaussian fit.

4.6. AFM at SMD

The AFM measurements were performed on a DI3100 instrument. The traceability to the meter was achieved by a calibration using two step height standards (VLSI STS3-440P and STS3-1800P), calibrated by comparison to NIST 821/261555–99 reference standard. All the measurements were performed in a conditions-controlled laboratory.

The deposition procedure was similar to the one used at METAS, except that poly-L-lysine was used to fix all the nanoparticles. The dilution was chosen in order to have isolated nanoparticles on the mica surface; it varied between 10^3 and 10^5-fold. The scan speed was set to 0.5 Hz, the amplitude setpoint was set at maximum 85% of the free amplitude (light tapping). The tips were standard silicon tips for tapping measurement in air (40 N m^{-1}, 300 kHz). The diameter of the particles was determined the same way as described by METAS. Figure 7 shows a typical AFM measurement and a typical size evaluation result.

For the bimodal distribution, the histograms were fitted with a Gaussian curve in order to extract the mean values for the two size fractions.

In the second part of the stability experiment an improved measurement uncertainty evaluation was applied, including the variability caused by different operators and image analysts. Other major contributions to the measurement uncertainty were the vertical calibration using step height standards, and the uncertainty associated to the background level of the images (poly-L-lysine background).

4.7. AFM at VSL

The diameter of the nanoparticles was determined as the height of the particles with respect to a mica substrate using AFM. A commercial AFM (VEECO Dimension 3100) was operated in tapping mode using standard silicon cantilevers (spring constant 10 N m^{-1}, resonance frequency 140 kHz). The z-axis

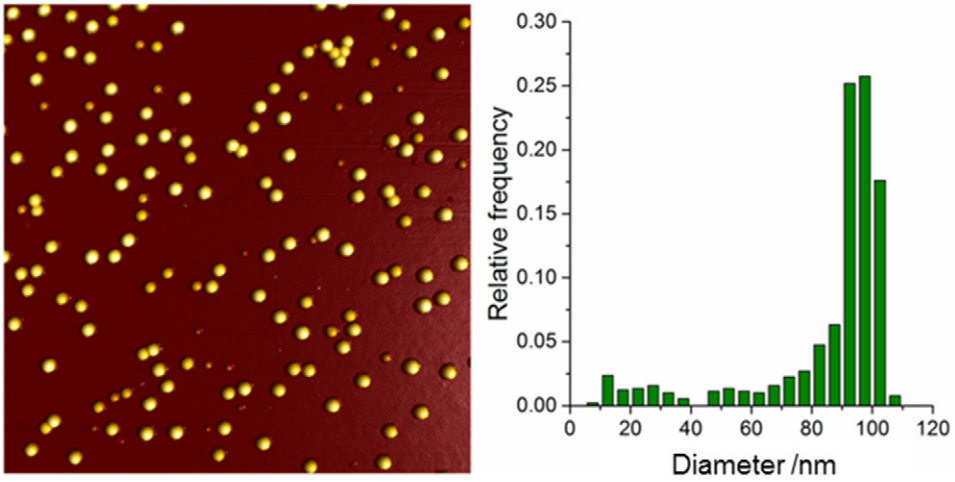

Figure 8. Typical AFM image (4.5 μm × 4.5 μm) of the sample PS_100 (table 1) on a mica substrate as obtained by VSL (left) and the corresponding size distribution (right).

of the AFM was calibrated using step height standards. The standards were calibrated using an interference microscope equipped with a mercury discharge lamp whose traceable 546 nm line was used. The interference microscope was validated by participating in the nano2 comparison (CCL-S2) [31].

The sample preparation, the AFM imaging strategy, the analysis and the evaluation of the measurement uncertainty were similar to the aforementioned approach of METAS, with one major exception. The dilution factor of a particular sample (typically between 100 and 400-fold) and the exposure time of the sample to the poly-L-lysine treated mica were chosen such that the number of single particles on the substrate was maximized, with a reasonable separation between the particles to accurately determine the local height of the background. Clusters of particles were not taken into account for the analysis. Although it was not expected that clustering substantially influences the apparent height of the particles in the cluster, it was unknown if such an effect is completely absent for the samples in this comparison. Figure 8 shows the results of the sample PS_100.

5. General comparison definitions and requirements

The measurand in this comparison was defined to be the mean diameter of the particles contained in each sample sent to the participants. A single particle diameter represents the diameter of a perfect sphere having the same volume as the particle. The diameter to be reported by the participants was defined as the arithmetic mean of the individual particle diameters of all particles analysed (number-weighted mean diameter, equation (1)).

$$d_{\text{mean}} = \frac{1}{n}\sum_{i=1}^{n} d_i. \tag{1}$$

Besides the arithmetic mean diameter, additional particle information such as the number of particles analysed, the standard deviation of the distribution and if possible, the mode value (highest probability value) and the particle size distribution were requested.

For the bimodal samples the mean diameter of each size fraction and the mean diameter of the overall distribution were determined. Additionally, the number of particles analysed in each fraction and the standard deviations for both size fractions were required.

The measurement uncertainties were calculated using all known influences such as contributions from particle shape, particle size distribution, sampling of the material, sample preparation and all contributions specific for the measurement method as well as possible deviations from the measurand definition. For the clinical methods PTA and RPS no uncertainty estimation based on fundamental influence factors was made.

6. Comparison evaluation

The comparison reference value (x_{ref}) for each sample was calculated as the weighted mean of the measurements (x_i) (equation (2)). The weights were $u^{-2}(x_i)$. The standard uncertainty $u_c(x_{\text{ref}})$ of the reference value was calculated according to equation (3) [32].

$$x_{\text{ref}} = \frac{\sum_{i=1}^{n} u^{-2}(x_i)\cdot x_i}{\sum_{i=1}^{n} u^{-2}(x_i)} \tag{2}$$

$$u_c(x_{\text{ref}}) = \left(\sum_{i=1}^{n} u^{-2}(x_i)\right)^{-1/2}. \tag{3}$$

The expanded uncertainty with a confidence level of 95% (U_{95}) was estimated using an expansion factor $k_{95} = 2$ (equation (4)).

$$U_{95}(x_{\text{ref}}) = u_c(x_{\text{ref}})\cdot k_{95}. \tag{4}$$

6.1. Tests of consistency

The consistency of an individual measurement result with the corresponding reference value was verified using the

Table 5. Participants values for the mean diameter (mode for PS_100) of the monodisperse samples and the standard uncertainties u_c ($k = 1$). In the last row the reference values with their standard uncertainties computed from five independent methods are given. The non-consistent values are marked with an asterisk(*). All values in nm.

		SiO_2_255		SiO_2_48		PS_315		PS_147		PS_100	
Laboratory	Method	Mean	u_c	Mean	u_c	Mean	u_c	Mean	u_c	Mode	u_c
AMC	RPS	291.4	NA	104.6	NA	318.7	NA	150.7	NA	105.0	NA
AMC	PTA	243.9	NA	86.6	NA	313.4	NA	145.4	NA	95.0	NA
PTB	TSEM	255.6	2.4	53.6	1.0	319.3	3.2	145.0	2.1	102.9	2.8
PTB	SAXS	252.1	3.5	57.6*	0.8	312.2	4.4	147.0	4.7	101.3	2.8
VSL	AFM	261.0	3.3	53.5	2.2	311.7	3.0	145.6	2.1	97.5	2.1
SMD	AFM	251.8	4.3	64.6*	2.9	319.9	8.0	134.2	9.4	93.0	7.5
METAS	AFM	247.5	3.2	53.3	1.2	305.0	3.6	140.3	2.4	94.5	2.2
Reference value		254.0	1.4	53.5	0.7	312.8	1.7	144.0	1.2	98.2	1.2

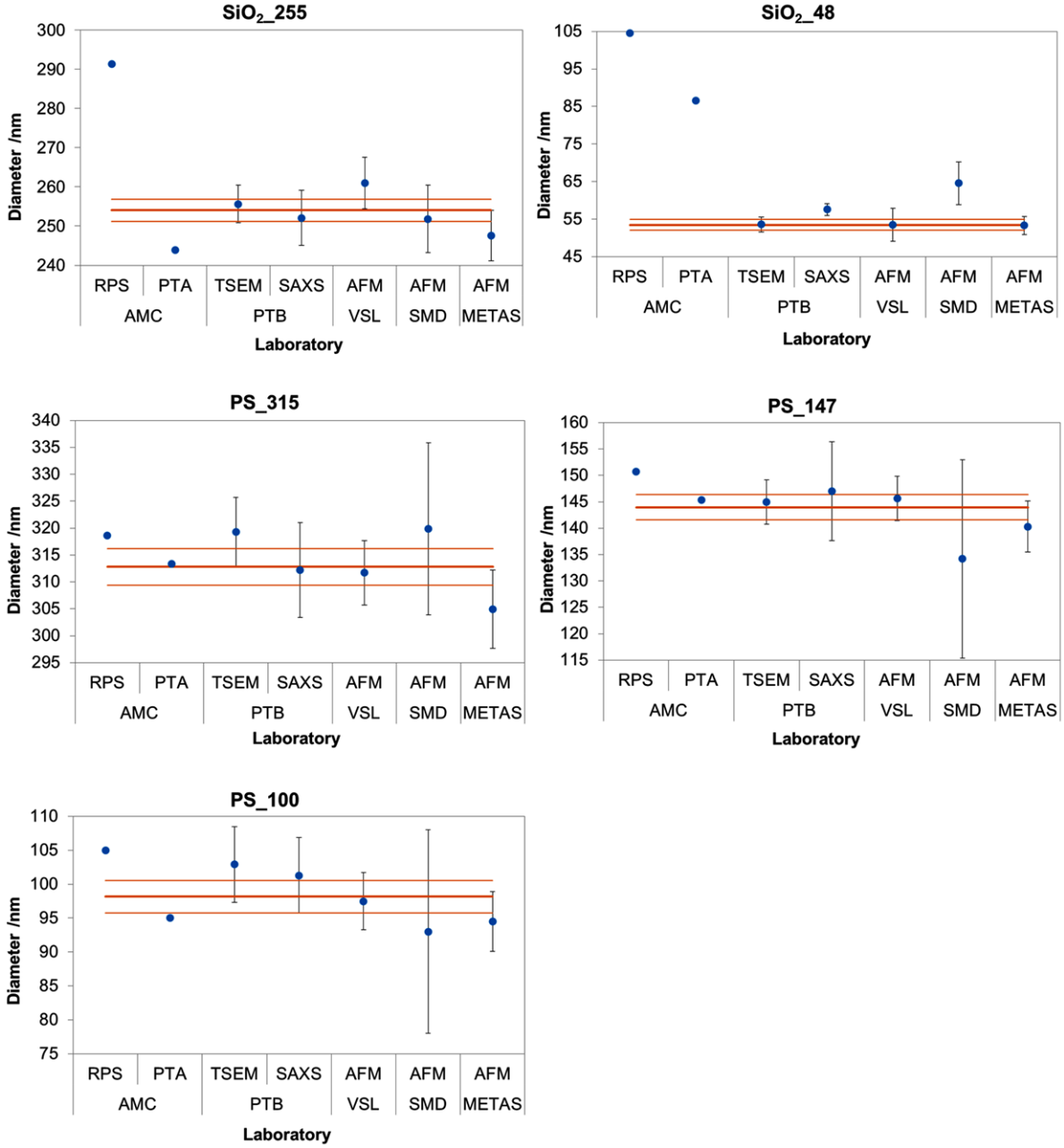

Figure 9. Monodisperse particle mean size values with expanded uncertainty ($k = 2$) for all samples except for the sample PS_100 where the mode values are shown. The thick straight line is the reference value, and the two thin lines indicate the uncertainty range ($k = 2$). See table 1 for a more detailed description of the samples.

Table 6. Absolute differences and agreements (expressed as En_{95} values (equation (5))) of the measured values to the reference values.

		SiO_2_255		SiO_2_48		PS_315		PS_147		PS_100	
Laboratory	Method	Diff (nm)	En_{95}	Diff (nm)	En_{95}	Diff (nm)	En_{95}	Diff (nm)	En_{95}	Diff (nm)	En_{95}
AMC	RPS	37.4	NA	51.1	NA	5.9	NA	6.7	NA	6.8	NA
AMC	PTA	−10.1	NA	33.1	NA	0.6	NA	1.4	NA	−3.2	NA
PTB	TSEM	1.6	0.4	0.1	0.1	6.5	1.2	1.0	0.3	4.7	0.9
PTB	SAXS	−1.9	−0.3	4.1	1.9	−0.6	−0.1	3.0	0.3	3.1	0.6
VSL	AFM	7.0	1.2	0.0	0.0	−1.1	−0.2	1.6	0.5	−0.7	−0.2
SMD	AFM	−2.2	−0.3	11.1	1.9	7.1	0.5	−9.8	−0.5	−5.2	−0.3
METAS	AFM	−6.5	−1.1	−0.2	−0.1	−7.9	−1.2	−3.7	−0.9	−3.7	−1.0

En_{95} value. The En_{95} value is the ratio between the deviation from the reference value and the uncertainty of this difference (equation (5)) at a confidence level of 95% ($k = 2$). The minus sign ('−') is used in the denominator for values contributing to the reference value and a plus sign ('+') for values not contributing to the reference value in order to account for correlation. $|En_{95}| > 1$ indicates possible inconsistency.

$$En_{95}(d_i) = \frac{d_i - d_{\mathrm{ref}}}{2 \cdot \sqrt{u_c^2(d_i) \mp u_c^2(d_{\mathrm{ref}})}}. \quad (5)$$

The Birge criterion was used to verify that measurements were consistent [33]. In the case of inconsistent results the one with the largest *En* value was excluded until the largest consistent subset was found which fulfils the Birge criterion. Results not contributing to the reference value were marked with an asterisk in the tables 5, 7 and 8. Out of 55 results 6 were excluded.

The particle samples with the estimated reference values will be used to verify and compare further EVs measurements. Thus the main goal of this inter-laboratory comparison was not the validation of the individual participant's results, but the estimation of a reliable reference value for the distributed particle samples.

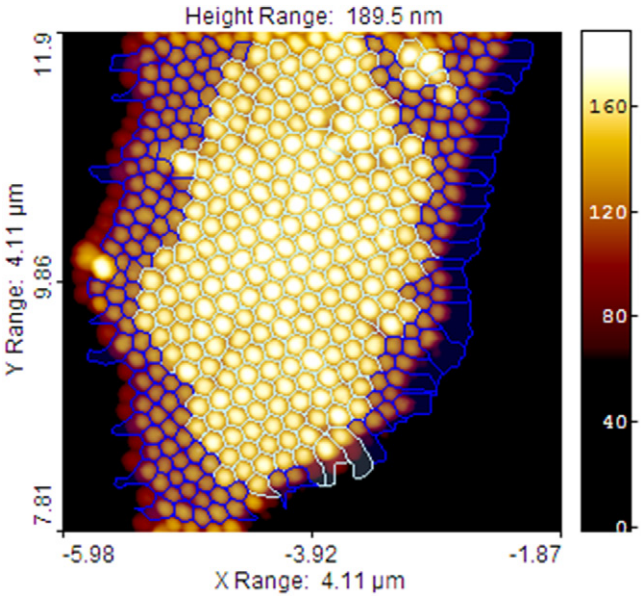

Figure 10. AFM image measured by METAS of the bimodal silica sample SiO_2_bim (table 2) showing segregation. Larger particles are light coloured and concentrated in the middle of the island while the smaller fraction is dark coloured and located at the border of the island. Image size 4.11 μm × 4.11 μm, 512 × 512 pixels. Image evaluation with SPIP.

7. Results

Four national metrology institutes and a university hospital provided results from seven different measurement systems representing five different methods.

7.1. Monodisperse samples results

The received results are summarized in table 5, showing the measured mean values and uncertainties together with the computed reference values and respective uncertainties. Because of the non-symmetric size distribution of sample PS_100 (table 1), see also figures 5 and 8, the mode values were used here instead of the mean values. Reference values were calculated for each sample using equation (2). The reference values were calculated including all consistent results, which were supplied with an uncertainty estimation. For the methods with single particle analysis from microscope images, such as AFM and TSEM, the number of particles analysed is an important indicator of the quality of a measurement. VSL-AFM analysed more than 80 particles per size and SMD-AFM about 700. METAS-AFM analysed over 1500 particles per sample and PTB-TSEM over 4000. Furthermore the image locations were randomly selected; the result is thus a good representation of the sample. For the other methods (SAXS, PTA and RPS), the measurements are performed in liquid and some thousands of particles are measured.

In figure 9 the individual values and the reference values are shown with their respective uncertainty for a confidence level of 95% ($k = 2$) for all 5 monodisperse samples. PTA and RPS did not produce consistent results for the smallest 48 nm particles (SiO_2_48) where the measured diameters were much too large. A possible explanation could be the insensitivity to the small particles in this sample and the counting of particle clusters instead. In general the PTA results were always lower than the corresponding RPS values and the RPS values were for all samples clearly above the reference value.

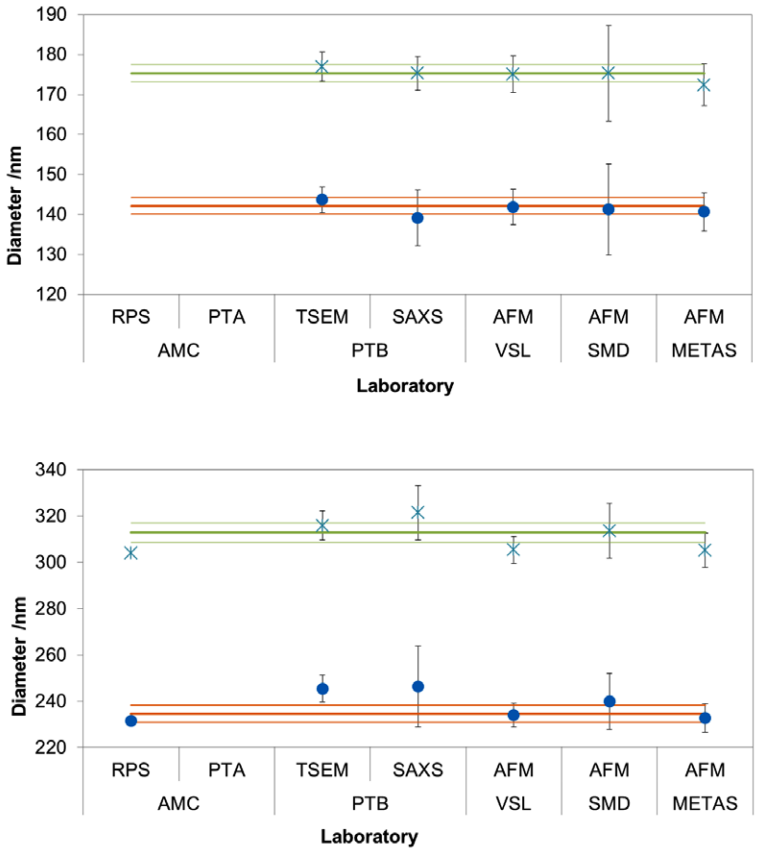

Figure 11. Particle mean size values with expanded uncertainty ($k = 2$) and reference values for the size fractions of the silica bimodal sample (top) and for the polystyrene bimodal sample (below). The thick straight lines are the reference values, and the two corresponding thin lines indicate the expanded uncertainties ($k = 2$).

The surface chemistry of the particles in the sample SiO_2_48 was different from standard SiO_2 particles (modified with functionalized carboxyl-chains) and the measured reference value deviates from the given nominal manufacturer value by much more than for the other samples (about 11%). This might be explained by the hybrid aspect of these particles. The SAXS measurement, with the particles measured in aqueous suspension, gave clearly a larger diameter value than the TSEM measurement obtained in vacuum. This might be an indication of particles shrinking upon drying.

The absolute difference and the agreement of the individual values with the reference value, expressed as En_{95} using equation (5), are shown in table 6. A reasonable agreement between the different measuring methods was found as the Birge criterion [33] was fulfilled for all monodisperse samples except for the above mentioned sample SiO_2_48. For both samples PS_147 and PS_100 all En_{95} absolute values were smaller than 1, indicating a good agreement. For the samples PS_315 and SiO_2_255 samples, some results have En_{95} absolute values slightly larger than 1, but the agreements were still reasonable as the Birge criterion was fulfilled. For the sample SiO_2_48 however, four En_{95} absolute values were larger than 1. In fact, the results of PTB-SAXS and SMD-AFM were not in agreement and had to be excluded to satisfy the Birge criterion. Alternatively, roughly a 2 nm higher uncertainty estimation would also lead to consistency. On the other hand there are indications that the SAXS measurement is correct and that the difference can be explained by sample shrinkage in air or vacuum for this special type of particle material, see table 1 and conclusions.

7.2. Bimodal samples results

Preparation of bi-, multimodal or other broad size distribution samples had to ensure that all sizes were equally represented in the sample to be analysed and that no segregation processes occurred or falsified the result. Indeed the smaller particles were more mobile than the bigger ones essentially due to a faster Brownian motion. In fact segregation was frequently observed on AFM samples (figure 10). In these cases AFM imaging had to make sure that all segregated fractions were equally represented in the measurements. Ensemble methods suffered less from this problem but here the sensitivities were often size dependent or as in the case of SAXS the size distribution must be modelled for the evaluation. The number of particles analysed for the microscopy techniques are similar to the monodisperse samples with some hundreds of particles analysed by VSL-AFM and SMD-AFM, 1500 particles by METAS-AFM and over 4000 particles by PTB-TSEM.

The diagrams in figure 11 show the mean diameter of each size fraction (d_1 and d_2) with the reference values and uncertainties of both bimodal samples. As the two size classes were clearly separated in the PS sample, the individual mean diameters could be easily evaluated with all methods except

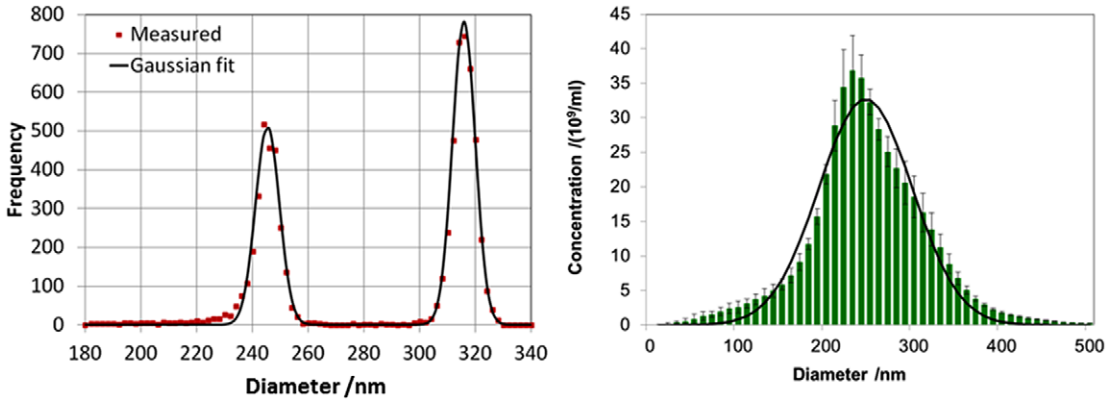

Figure 12. Size distribution for the bimodal polystyrene sample measured with TSEM (left) and PTA (right) shown with Gaussian fits. In this sample, the used particle fractions had a clear size difference, but PTA was not able to distinguish them.

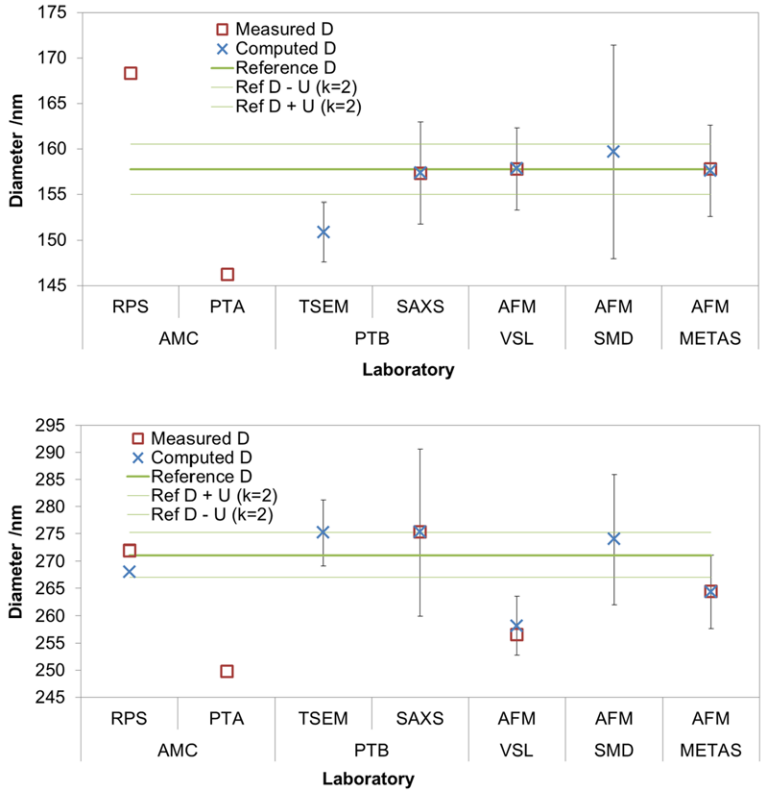

Figure 13. Particle mean size value with expanded uncertainty ($k = 2$) and reference values for the whole distribution of the silica bimodal sample (top) and the polystyrene bimodal sample (bottom). The thick straight line is the reference value, and the two thin lines are reference values with uncertainties ($k = 2$). The mean of all measured values (squares) are direct results from the participants while the computed values (crosses) are evaluated with the diameters of each size fraction weighted with the number of particles in each fraction (equation (6)).

PTA as illustrated in figure 12. In the sample SiO_2_bim, the particle size distributions of the two fractions overlapped slightly and the diameters were evaluated with the help of a double least-squared Gaussian curve fitted to the measured size distribution. The RPS and PTA methods were not able to distinguish the two size fractions in the sample SiO_2_bim. The reference values and respective uncertainties for each fraction were calculated as previously with equations (2) and (3) using all consistent measurements. To ensure consistency, the PTB-TSEM value and the VSL-AFM value were excluded for d_1, respectively d_2 of the polystyrene bimodal sample.

The measurements given with uncertainties were, after exclusion of these 2 values, in good agreement with the reference values at a confidence level of 95% ($\pm 2u$).

The overall mean size of the bimodal samples (D) depends on the size and number concentration of the particles in each fraction. The mean size value of a bimodal sample is therefore a way to test possible size dependent sensitivities of the methods. All participants provided the mean diameters of the two size fractions (d_1 and d_2) and the respective number or percentage of particles analysed (n_1 and n_2). Using these values, the overall mean size of a bimodal sample was then calculated as the weighted mean of the diameters of each

Table 7. Participant values for the three diameters (D, d_1 and d_2) of the silica bimodal sample and their respective combined standard uncertainties ($k = 1$). The diameter of the overall distribution (D) was calculated for all methods except for RPS and PTA where measured values are given. In the last column, the ratio between the particle number concentration of each fraction is shown. The reference values with their standard uncertainties are shown in the last row. The non-consistent value is marked with an asterisk(*).

		SiO_2_bim						
Laboratory	Method	*D* (nm)	*u_D* (nm)	*d1* (nm)	*u_d1* (nm)	*d2* (nm)	*u_d2* (nm)	*n2/n1*
AMC	RPS	168.3	NA	NA	NA	NA	NA	NA
	PTA	146.2	NA	NA	NA	NA	NA	NA
PTB	TSEM	150.9*	1.6	143.7	1.6	177.0	1.8	0.3
	SAXS	157.3	2.8	139.2	3.5	175.3	2.1	1.0
VSL	AFM	157.8	2.2	141.9	2.2	175.1	2.3	0.9
SMD	AFM	159.7	5.9	141.3	5.7	175.3	6.0	1.2
METAS	AFM	157.6	2.5	140.7	2.4	172.4	2.6	1.1
Reference value		157.7	1.4	142.2	1.1	175.4	1.1	—

fraction (equation (6)). For each size fraction, the uncertainties of the diameter values were stated by the participants but no uncertainties for the number of particles analysed were given. Because the systematic errors were for all methods the main uncertainty contributions it was assumed that the diameter values of the two size fractions were highly correlated. Based on this assumption and the available information the combined uncertainty of the overall mean size D was estimated as the uncertainty of two correlated results (equation (7)). No contribution due to the uncertainty of the relative number of particles analysed was included. For RPS and PTA no uncertainties were given at all and therefore these methods could not contribute to the reference value calculation of D. Some methods delivered also a value for D which was directly derived from all measured particles.

$$D = \frac{n_1 \cdot d_1 + n_2 \cdot d_2}{n_1 + n_2} \tag{6}$$

$$u_c(D) = \frac{n_1}{n_1 + n_2} \cdot u_{c,d_1} + \frac{n_2}{n_1 + n_2} \cdot u_{c,d_2}. \tag{7}$$

Figure 13 shows the mean diameter (D) of the whole bimodal distribution (calculated and measured), the reference value and the respective expanded uncertainty U_{95}. The values of the participants with the reference values are summarized in tables 7 and 8. The difference observed by AMC-RPS and VSL-AFM between the measured and the computed value of D for the polystyrene sample in figure 13 was due to the evaluation method. Measured D was the arithmetic mean value of all the particles analysed, while computed D was dependent on the values of n_1, n_2, d_1 and d_2, which were separately evaluated by the participants.

Most values of the methods capable of detecting the two size fractions agreed within the uncertainties. No uncertainty contribution for the respective number of particles analysed in each size fraction was considered and therefore the combined uncertainty of D was systematically too small. In fact the PTB-TSEM method indicated a rather small value for the ratio n_2/n_1 of the bimodal SiO_2 sample (table 7), i.e. less particles of the large size constituent than expected showed up as non-touching particles on the TEM grids. This imbalance influences the calculated mean size (equation (6)) which is thus not consistent with the reference mean (see figure 13 top). This value was thus excluded for the calculation of the reference value. Also for the sample PS_bim, the value of the VSL-AFM had to be excluded to lead to consistency.

One fraction in one of the bimodal samples was already used in the monodisperse particle comparison. These were in fact those of the PS_315 sample. The monodisperse sample reference value was (312.8 ± 1.7) nm and the value measured within the bimodal sample was (312.9 ± 2.1) nm. The two values agree well within the uncertainties. This is a clear indication that when mixing two sizes of particles the individual fraction size is maintained.

7.3. Long-term stability results

Six samples were measured again 12 or 18 months later in order to evaluate the long-term stability. During storage the samples were kept at normal laboratory conditions with temperatures around 20 °C. Using all results from the participants, new weighted reference values were calculated with consistent results and compared with the initial reference values. Due to the rather broad size distribution of sample PS_100 it was not measured again. Because of improved or recalibrated instruments and partly modified measurement procedures, it was difficult to determine a specific uncertainty for a diameter change, which considers the correlation between the initial and the final measurements. Therefore, the correlation was neglected and the uncertainty of the diameter change was calculated as the combined uncertainty of two independent measurements.

The initial and final reference values with uncertainties and absolute differences of the final measurements to the initial measurements with their uncertainties are shown in table 9 for the monodisperse samples and in table 10 for the bimodal samples.

Figure 14 shows the diameter changes during the long-term storage together with the estimated uncertainties ($k = 2$).

For the monodisperse samples, all measured diameter differences were smaller than the expanded uncertainties at a confidence level of 95% ($\pm 2u$), i.e. the diameter change lies within the measurement uncertainty. This confirms a good

Table 8. Participant values for the three diameters (D, d_1 and d_2) of the polystyrene bimodal sample and their respective combined standard uncertainties ($k = 1$). The diameter of the overall distribution (D) was calculated for all methods except for RPS and PTA where measured values are given. In the last column, the ratio between the particle number concentration of each fraction is shown. The reference values with their standard uncertainties are shown in the last row. The non-consistent values are marked with an asterisk(*).

		PS_bim						
Laboratory	Method	D (nm)	u_D (nm)	$d1$ (nm)	u_d1 (nm)	$d2$ (nm)	u_d2 (nm)	$n2/n1$
AMC	RPS	271.9	NA	231.6	NA	303.9	NA	1.0
	PTA	249.8	NA	NA	NA	NA	NA	NA
PTB	TSEM	275.2	3.0	245.4*	2.9	315.9	3.2	0.7
	SAXS	275.3	7.7	246.3	8.8	321.4	5.9	0.6
VSL	AFM	258.1*	2.7	233.9	2.6	305.4*	2.9	0.5
SMD	AFM	274.0	6.0	239.9	6.0	313.6	5.9	0.9
METAS	AFM	264.4	3.4	232.7	3.1	305.1	3.7	0.8
Reference value		271.1	2.0	234.6	1.8	312.9	2.1	-

Table 9. Reference values and uncertainties for the initial and final measurements of the monodisperse samples and the corresponding diameter changes.

	d_i (nm)	u_i (nm)	d_f (nm)	u_f (nm)	$\Delta f - i$ (nm)	u_Δ (nm)	$\Delta f - i / u\_\Delta$
SiO_2_255	254.0	1.4	252.1	1.6	−1.9	2.1	−0.9
SiO_2_48	53.5	0.7	54.0	0.7	0.5	1.0	0.5
PS_315	312.8	1.7	312.1	2.0	−0.7	2.6	−0.3
PS_147	144.0	1.2	142.1	1.2	−1.9	1.7	−1.1

Table 10. Reference values and uncertainties for the initial and final measurements of the bimodal samples and the corresponding diameter changes.

		d_i (nm)	u_i (nm)	d_f (nm)	u_f (nm)	$\Delta f - i$ (nm)	u_Δ (nm)	$\Delta f\text{-}i / u\_\Delta$
SiO_2_bim	d1	142.2	1.1	142.3	1.2	0.2	1.6	0.1
	d2	175.4	1.1	174.4	1.0	−0.9	1.5	−0.6
	D	157.7	1.4	156.2	1.1	−1.6	1.8	−0.9
PS_bim	d1	234.6	1.8	237.7	2.2	3.1	2.8	1.1
	d2	312.8	2.1	314.9	1.8	2.0	2.8	0.7
	D	271.1	2.0	276.1	1.8	5.0	2.7	1.8

stability of both the SiO_2 and PS particle samples and a possible deterioration within the time span of the investigation cannot be proven.

For the bimodal samples the measured diameter differences were also smaller than the expanded uncertainties ($k = 2$). A slight trend towards smaller values could be observed for the monodisperse samples but this was not confirmed by the bimodal samples. Thus a third analysis some years later would be required to confirm if this was a trend.

An upper limit for a possible diameter change with time could be given using all results obtained so far. Using the initial and the final reference values with their respective uncertainties an upper limit for a possible diameter change of 3.1% yr^{-1} for the monodisperse samples made of SiO_2 and 2.4% for the PS sample, 3.2% yr^{-1} for SiO_2 and 3.8% yr^{-1} for PS particles in the bimodal samples can be given.

8. Discussion and conclusion

We have performed an inter-laboratory comparison on the size and stability of five monodisperse and two bimodal synthetic reference particles samples for standardization of EV measurements. PS and SiO_2 particles in the size range of EV were analysed by metrologically traceable methods and non-traceable clinical laboratory methods to study their accuracy in sizing and relative counting, and also to study the particle stability.

All NMI methods (AFM, TSEM, SAXS) agreed within the specified size uncertainties for the high quality monodisperse samples. The samples with less agreement were either small (<50 nm) or less monodisperse. Here discrepancies could be due to the presence of small fractions of particles that deviate from the mean size. Due to implicit or explicit size limits applied during the particle size evaluation, deviations could be introduced, which were typically not considered in the uncertainty calculation. Often discussed influences, such as the particle material, surrounding environment (water, air or vacuum), particle charging, particle deformation by adhesion or probing forces, could not be identified. Only for the sample SiO_2_48 (hybrid) there was an indication of particle shrinkage upon drying.

For bimodal samples made by mixing high quality monodisperse particle suspensions the NMI methods agreed almost within the specified size uncertainties of the subpopulations.

Due to size selective sample preparation, lack of an uncertainty contribution for the relative number of particles in each size fraction, possibly size dependent sensitivities and different size detection limits of methods, particle size comparisons for bimodal samples were more difficult compared to monodisperse samples. Continued systematic comparisons of bimodal samples could be a promising way for further investigations, since it may bridge the gap between traceable measurements of monodisperse samples and hitherto untraceable measurements on EV and other samples with broad size distribution [6].

Unlike the NMI methods, the clinical laboratory methods (RPS and PTA) have no calculable uncertainty and they are often calibrated using monodisperse PS beads provided by the manufacturers. To determine their size accuracy, the detected mean sizes were compared to the mean size of the NMI methods. For the monodisperse PS beads, RPS and PTA deviated on average only 6.5 nm (about 3%) and 1.7 nm (0.6 %) from the NMI determined reference values. However, for the SiO_2_255 beads, the deviation was 37 nm (15%) for RPS and 10 nm (4%) for PTA, which was unacceptably high for a clinical instrument. For RPS, we hypothesize that this high deviation may be caused by changes in the nanopore dimensions between the measurement and the calibration, especially because the nanopore is made from polyurethane, which is a flexible material. Furthermore, both RPS and PTA overestimated the mean size of the SiO_2_48 beads up to 96%. Most likely, these beads were below the detection limit and aggregates were measured instead. In this case, RPS and PTA should have provided a warning instead of an incorrect result.

Traceable long-term stabilities of reference particles were determined in this study. No indication of instability was found for the evaluation period of 18 months. Upper limits for particle size changes, including the measurement uncertainties, were in the order of 3% yr^{-1} for the monodisperse samples. Continued monitoring of these samples would probably even lower this limit.

In conclusion, the NMI methods AFM, TSEM, SAXS, used for size measurements, agreed to a large extent within the specified uncertainties for high quality monodisperse and bimodal samples. This is a useful contribution to the roadmap of the standardization of EV measurements. Knowledge of the size distribution of the reference materials is not only valuable for size calibration, but also a prerequisite for determining the particle number concentration from the mass density of the particles. Moreover, owing to their low refractive index, SiO_2 beads resemble the optical properties of EV better than PS beads and present currently the optimal choice for the calibration of EV measurements. In addition, measurements of the bimodal samples may be a step towards the development and characterization of polydisperse reference materials and eventually a fully traceable size determination of EV. Finally, we conclude that currently used clinical laboratory methods, such as RPS and PTA, perform well on sizing PS beads within their detection range, but that data requires careful interpretation for other samples.

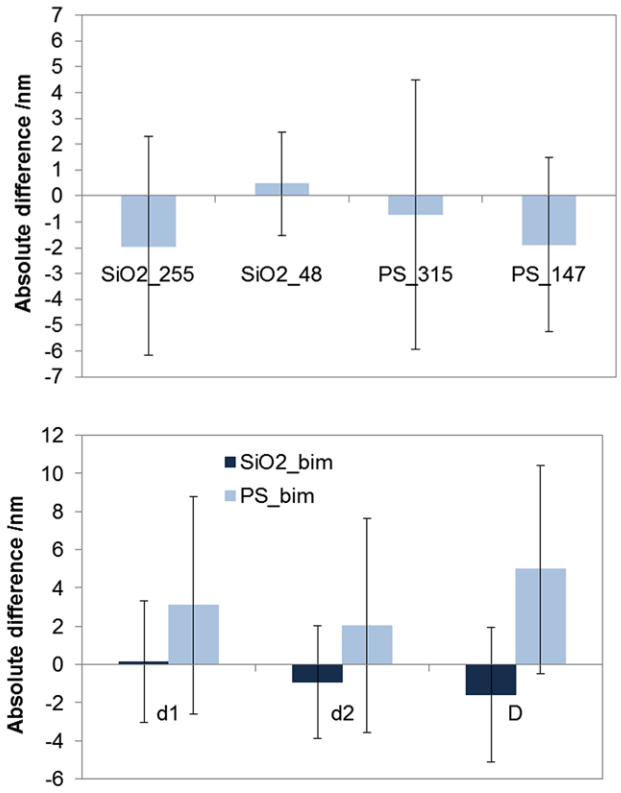

Figure 14. Mean diameter changes during the time span of the long-term stability measurements with respect to the initial measurement given with the combined uncertainty ($k = 2$) for the monodisperse (top) and the bimodal (bottom) samples.

Acknowledgments

This work is part of the EMRP project 'Metrological Characterization of microvesicles as biomarker'. The project is jointly funded by the EMRP participating countries within EURAMET and the European Union.

References

[1] van der Pol E, Böing A N, Harrison P, Sturk A, Nieuwland R 2012 Classification, functions, and clinical relevance of extracellular vesicles *Pharmacol. Rev.* **64** 676–705
[2] van der Pol E *et al* 2014 Particle size distribution of exosomes and microvesicles determined by transmission electron microscopy, flow cytometry, nanoparticle tracking analysis and resistive pulse sensing *J. Thromb. Haemost.* **12** 1182–92
[3] van der Pol E, Hoekstra A G, Sturk A, Otto C, van Leeuwen T G and Nieuwland R 2010 Optical and non-optical methods for detection and characterization of microparticles and exosomes *J. Thromb. Haemost.* **8** 2596–607
[4] van der Pol E, Coumans F A W, Sturk A, Nieuwland R and van Leeuwen R G 2014 Refractive index determination of nanoparticles in suspension using nanoparticle tracking analysis *Nano Lett.* **14** 6195–201
[5] Varga Z, Yuana Y, Grootemaat A E, van der Pol E, Gollwitzer C, Krumrey M and Nieuwland R 2014 Towards traceable size determination of extracellular vesicles *J. Extracellular Vesicles* **3** 23298

[6] Mulholland G W, Bryner N P and Croarkin C 1999 Measurement of the 100 nm NIST SRM 1963 by differential mobility analysis *Aerosol Sci. Technol.* **31** 39–55
[7] Germer T A, Mulholland G W, Kim J H and Ehrman S H 2002 Measurement of the 100 nm NIST SRM® 1963 by laser surface light scattering *Proc. SPIE* **4779** 60–71
[8] Jung K Y *et al* 2002 Measurement of 100-nm polystyrene sphere by transmission electron microscope *Powder Technol.* **126** 255–65
[9] Ehara K, Takahata K and Koike M 2006 Absolute mass and size measurement of monodisperse particles using a modified Millikan's method: II. Application of electro-gravitational aerosol balance to polystyrene latex particles of 100 nm to 1 μm in average diameter *Aerosol Sci. Technol.* **40** 521–35
[10] Meli F, Klein T, Buhr E, Frase C G, Gleber G, Krumrey M, Duta A, Duta S, Korpelainen V, Bellotti R, Picotto G B, Boyd R and Cuenat A 2012 Traceable size determination of nanoparticles, a comparison among European metrology institutes *Meas. Sci. Technol.* **23** 125005
[11] Fu W H 2012 Supplementary comparison on nanoparticle size, APMP comparison draft A private communication from CMS/ITRI, Hsinchu, Taiwan
[12] Wang C Y, Pan S P, Peng G S and Tsai J H 2005 A comparison study on the measurement of nanoparticles *Proc. SPIE* **5879** 323–8
[13] Wang C Y, Fu W E, Lin H L and Peng G S 2007 Preliminary study on nanoparticle sizes under the APEC technology cooperative framework *Meas. Sci. Technol.* **18** 487–95
[14] Microparticles GmbH, Volmerstr. 9A, D-12489 Berlin, http://microparticles.de/eigenschaften (accessed 27 January 2016)
[15] Anderson W, Kozak D, Coleman V A, Jämting A K and Trau M 2013 A comparative study of submicron particle sizing platforms: accuracy, precision and resolution analysis of polydisperse particle size distributions *J. Colloid Interface Sci.* **405** 322–30
[16] Motzkus C *et al* 2013 Size characterization of airborne SiO_2 nanoparticles with on-line and off-line measurement techniques: an interlaboratory comparison study *J. Nanopart. Res.* **15** 1919
[17] Nicolet A and Meli F Report on the needs specifications and commercial sources of microvesicle reference materials PDF-form available on www.metves.eu (accessed 27 January 2016)
[18] Izon Science Ltd, Christchurch, New Zealand www.izon.com/ (accessed 27 January 2016)
[19] Coumans F A, van der Pol E, Böing A N, Hajji N, Sturk G, van Leeuwen T G and Nieuwland R 2014 Reproducible extracellular vesicle size and concentration determination with tuneable resistive pulse sensing *J. Extracell. Vesicles* **3** 25922
[20] Van Der Pol E, Coumans F, Varga Z, Krumrey M and Nieuwland R 2013 Innovation in detection of microparticles and exosomes *J. Thromb. Haemost.* **11** 36–45
[21] Wernecke J *et al* 2014 Characterization of an in-vacuum PILATUS 1M detector *J. Synchrotron Radiat.* **21** 529–536
[22] Krumrey M and Ulm G 2001 High-accuracy detector calibration at the PTB four-crystal monochromator beamline *Nucl. Instr. Meth. A Proc. 7th Int. Conf. on Synchrotron Radiation Instrumentation* vol 467–467 pp 1175–8
[23] Minelli C, Garcia-Diez R, Sikora A E, Gollwitzer C, Krumrey M and Shard A G 2014 Characterization of IgG-protein-coated polymeric nanoparticles using complementary particle sizing techniques *Surf. Interface Anal.* **46** 663–7
[24] Hughes I and Hase T 2010 *Measurements and their Uncertainties: a Practical Guide to Modern Error Analysis* (Oxford: Oxford University Press) ISBN 9780199566327
[25] Buhr E, Senftleben N, Klein T, Bergmann D, Gnieser D, Frase C G and Bosse H 2009 Characterization of nanoparticles by scanning electron microscopy in transmission mode *Meas. Sci. Technol.* **20** 084025
[26] Klein T, Buhr E, Johnsen K P and Frase C G 2011 Traceable measurement of nanoparticle size using a SEM in transmission mode (TSEM) *Meas. Sci. Technol.* **22** 094002
[27] Klein T, Buhr E and Frase C G 2012 TSEM—a review of scanning electron microscopy in transmission mode and its applications *Advances in Imaging and Electron Physics* vol 171, ed P Hawkes (Amersterdam: Academic Press) pp 297–356
[28] Buhr E, Michaelis W, Diener A and Mirandé W 2007 Multi-wavelength VIS/UV optical diffractometer for high-accuracy calibration of nano-scale pitch standards *Meas. Sci. Technol.* **18** 667–74
[29] Chernoff D A, Buhr E, Burkhead D L and Diener A 2008 Picometer-scale accuracy in pitch metrology by optical diffraction and atomic force microscopy *Proc. SPIE* **6922** 69223J
[30] Johnsen K P, Frase C G, Bosse H and Gnieser D 2010 SEM image modeling using the modular Monte Carlo model MCSEM *Proc. SPIE* **7638** 76381O
[31] Koenders L *et al* 2003 Comparison on Nanometrology: Nano 2—Step height *Metrologia* **40** 04001
[32] Kacker R, Datla R and Parr A 2002 Combined result and associated uncertainty from interlaboratory evaluations based on the ISO Guide *Metrologia* **39** 279–93
[33] Birge R T 1932 The calculation of errors by the method of least squares *Phys. Rev.* **40** 207–27